

DOI: 10.1002/pc.28200

# RESEARCH ARTICLE







# Highly lubricating and wear-resistant Ti<sub>3</sub>C<sub>2</sub>T<sub>x</sub>@SiO<sub>2</sub>/PI composites based on the action of transfer film at the friction surface

Accepted: 24 January 2024

Guojing Chen | Zhenqian Ma | Shuai Jiang | Xinrui Wang | Yufei Huang | Chunpeng Chai 🗅

School of Materials Science and Engineering, Beijing Institute of Technology, Beijing, China

#### Correspondence

Chunpeng Chai, School of Materials Science and Engineering, Beijing Institute of Technology, Beijing 100081, China. Email: chaicp@bit.edu.cn

# Abstract

Polyimide (PI) is a special engineering plastic, widely involved in mechanical components, instruments, and petrochemicals. However, single PI material is inevitably subject to wear and tear in practice, which leads to weakened material properties. In this work, Ti<sub>3</sub>C<sub>2</sub>T<sub>x</sub>@SiO<sub>2</sub> was prepared to enhance the wear resistance and lubrication properties of PI by intercalating SiO2 into the interlayer of Ti<sub>3</sub>C<sub>2</sub>T<sub>x</sub> sheets. Ti<sub>3</sub>C<sub>2</sub>T<sub>x</sub>@SiO<sub>2</sub>/PI composites were fabricated in two steps to test the tribological performances. SiO<sub>2</sub> particles change the form of interfacial friction from sliding to rolling, thus relieving direct friction between material and steel ball. So, the composites have a minimum COF (COF = 0.33) when the content of Ti<sub>3</sub>C<sub>2</sub>T<sub>x</sub>@SiO<sub>2</sub> is 0.80 wt%. Moreover, the average value of wear rate was  $0.24 \times 10^{-5} \text{ mm}^3/(\text{N} \cdot \text{m})$  when  $\text{Ti}_3\text{C}_2\text{T}_x \otimes \text{SiO}_2$  content was 1.60 wt%, which was 91.0% lower compared to the PI matrix. During the friction process, the abrasive chips of the material migrate to the surface of the steel ball to form a transfer film, which protects the material and thus reduces the wear rate. Therefore, the hybrids Ti<sub>3</sub>C<sub>2</sub>T<sub>x</sub>@SiO<sub>2</sub> are effective and important wearresistant agents and solid lubricants to improve the wear resistance and lubricity of PI or other polymer materials.

# Highlights

- SiO<sub>2</sub> insert Ti<sub>3</sub>C<sub>2</sub>T<sub>x</sub> is a key factor in changing sliding friction into rolling friction, effectively reducing the COF.
- The average wear rate was 91.0% lower than that of the polyimide matrix when  $Ti_3C_2T_x@SiO_2$  content was 1.60 wt%.
- The minimum COF of Ti<sub>3</sub>C<sub>2</sub>T<sub>x</sub>@SiO<sub>2</sub>/PI composites reached 0.33 when the content of Ti<sub>3</sub>C<sub>2</sub>T<sub>x</sub>@SiO<sub>2</sub> was 0.80 wt%.
- The transfer film effectively reduces further wear of the material during friction.

# KEYWORDS

coefficient of friction, lubricity, polyimide, Ti<sub>3</sub>C<sub>2</sub>T<sub>x</sub>, Wear resistant

15480569, 0, Downloaded from https://4spepublications

s on line library. wiley. com/doi/10.1002/pc.28200 by BEJING INSTITUTION OF TECHNOLOGY, Wiley Online Library on [25/02/2024]. See the Terms and Conditions (https://online.

# 1 | INTRODUCTION

Polyimide (PI) is a commonly used engineering polymer material with low-temperature resistance, and excellent mechanical properties, widely involved in microelectronics, polymer coatings, aerospace, protective coatings for mechanical components, etc.<sup>1,2</sup> However, when polyimide is subjected to friction and wear, its properties deteriorate, making it difficult to meet the needs of the application.<sup>3</sup> The main strategy that has been reported to improve the friction properties of polyimide materials is to fill the polyimide matrix with wear-resistant reinforcement materials.<sup>4,5</sup> Common wear-resistant reinforcing materials include granules, rods, lamellae, and hybrids between them.<sup>6</sup> Lamellar reinforcements can provide lubricity to the polymer matrix through weak van der Waals forces between the layers. Common lamellar reinforcements include MoS2, BN, graphene, MXene, etc.<sup>7,8</sup> Especially, MXene is a 2D reinforcing material with abundant functional groups on the surface, which can interact well with other molecules through surface chemical modification.<sup>9,10</sup> MXene materials can be added to the polymer matrix to effectively improve the thermal and mechanical properties of the matrix, especially the tribological properties. Zhang et al. 11 filled Ti<sub>3</sub>C<sub>2</sub>T<sub>x</sub> into ultrahigh molecular weight polyethylene (UHMWPE) to explore the mechanical performance of UHMWPE. It was found that Ti<sub>3</sub>C<sub>2</sub>T<sub>x</sub> could act as a nucleation site to improve the crystallinity and surface hardness of UHMWPE. Du et al. 12 composited MXene with epoxy resin (EP) to investigate the friction performance of the samples, and the study revealed that MXene effectively enhanced the tribological properties of epoxy resin. Specifically, the COF of the composite containing 70 wt% MXene was 0.39 and the average wear rate was  $4.57 \times 10^{-4} \, \text{mm}^3/(\text{N} \cdot \text{m})$ . 0D particle intercalation is an effective way to reduce the COF of 2D materials. The particles can make 2D-layered materials with increased spacing making the layers easy to peel, which will improve the lubrication characteristics of the 2D material.  $^{14}$ 

SiO<sub>2</sub> particles with nanosphere structure are a typical 0D reinforcing material in the field of modified polymer tribological properties. 15 During the friction process, SiO<sub>2</sub> particles can act as rolling bearings, changing the type of friction of the polymer material from sliding friction to rolling friction, thus reducing the friction of the material. In addition, SiO<sub>2</sub> can also carry and transfer frictional stresses transferred from the polymer, thereby reducing the wear of the polymer material. 16,17 Zhang et al. 18 filled SiO<sub>2</sub> into the PI matrix and found that the composite with a modified SiO2 content of 10.0 wt% had superior wear resistance, with a 71.0% reduction in wear rate compared to PI. Therefore, the effect of hybrids made by depositing SiO<sub>2</sub> on Ti<sub>3</sub>C<sub>2</sub>T<sub>x</sub> nanosheets and interlayer deposition on the tribological properties of PI is a worthwhile investigation.

In this work,  $SiO_2$  was innovatively intercalated in situ between the  $Ti_3C_2T_x$  sheet layers to act as a rolling axis, which will allow the relative sliding of the  $Ti_3C_2T_x$ 

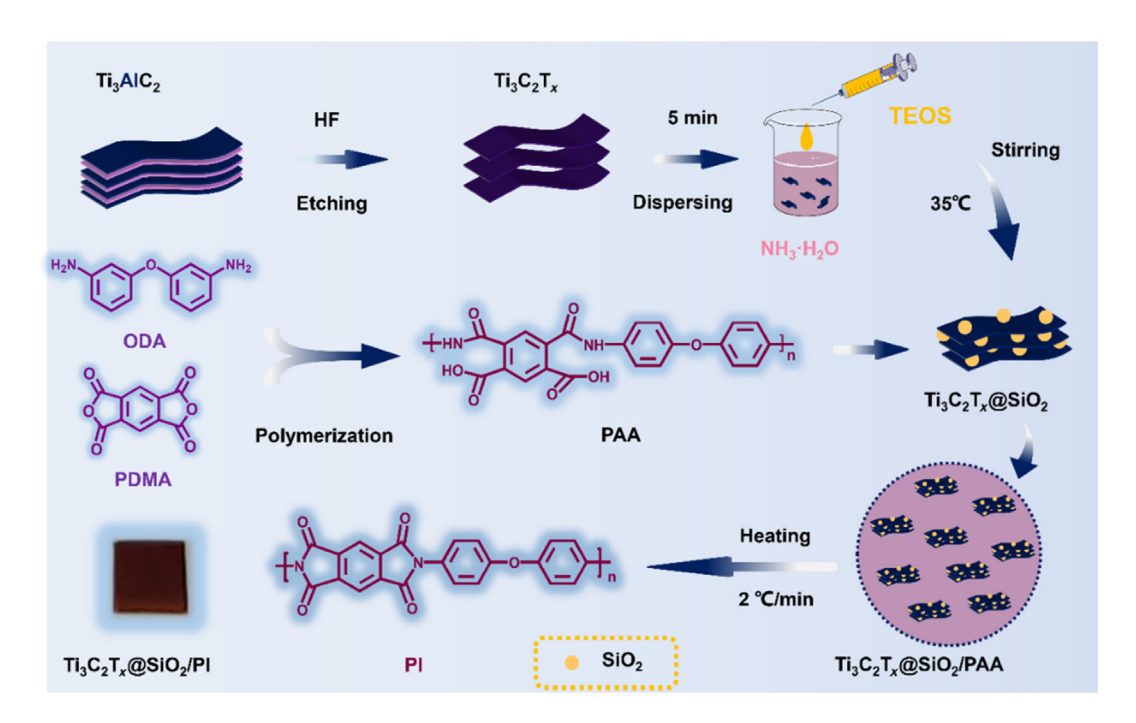
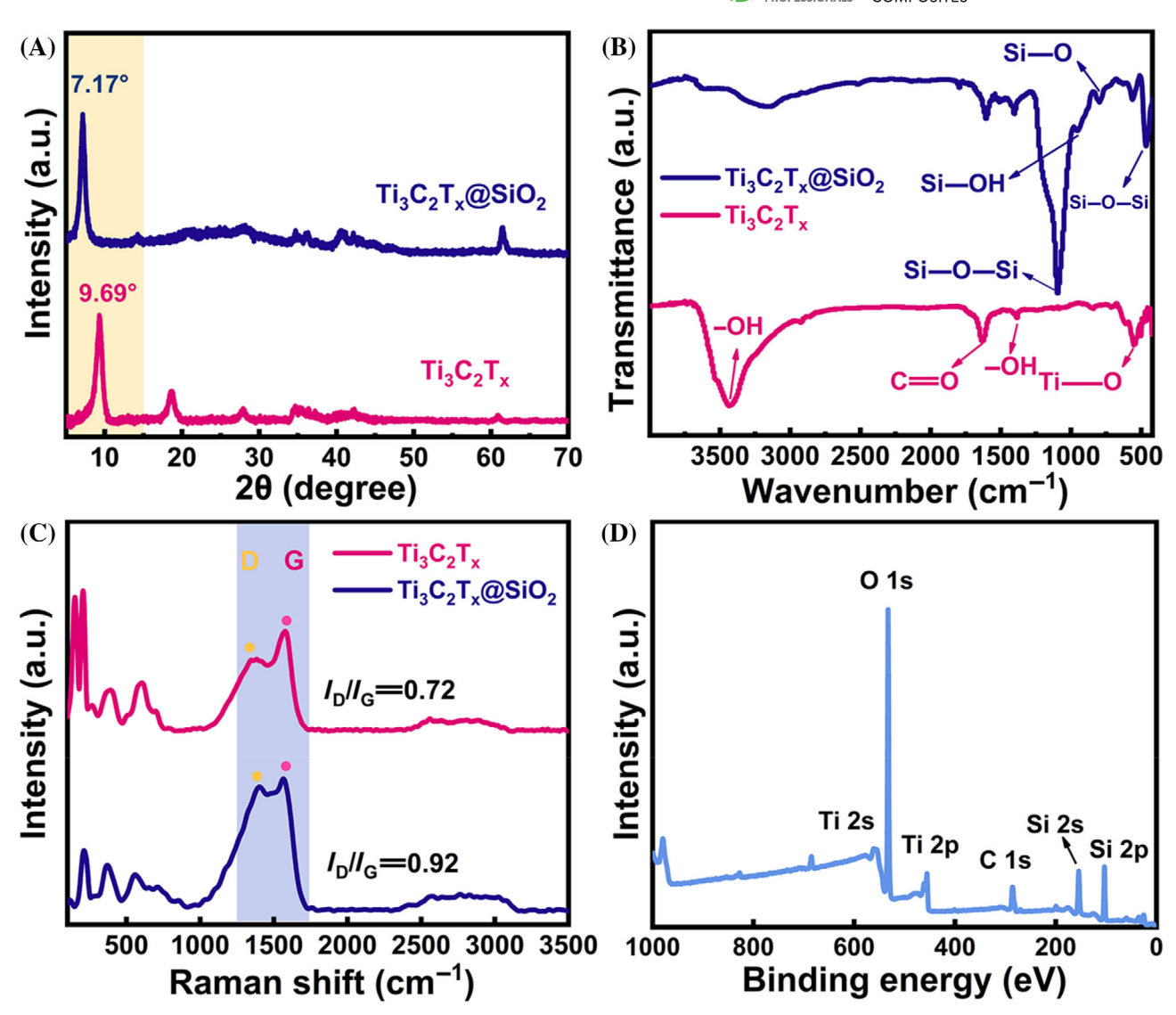


FIGURE 1 The process of preparing  $Ti_3C_2T_x@SiO_2/PI$  composites.

loi/10.1002/pc.28200 by BEIJING INSTITUTION OF TECHNOLOGY, Wiley Online Library on [25/02/2024]. See the Terr



**FIGURE 2** Chemical structure and component of  $Ti_3C_2T_x$  and  $Ti_3C_2T_x@SiO_2$ . (A) XRD image of samples. (B) FT-IR spectrum of samples (C) Raman analysis of samples. (D) XPS full spectrum of  $Ti_3C_2T_x@SiO_2$  sample.

sheet layers under frictional stress to be transformed into rolling, thereby increasing the lubrication. Therefore,  ${\rm Ti_3C_2T_x@SiO_2/PI}$  composites were prepared by filling  ${\rm Ti_3C_2T_x@SiO_2}$  hybrids into the PI matrix. The effect of  ${\rm Ti_3C_2T_x@SiO_2}$  on the thermal and tribological properties of polyimide substrates was analyzed in terms of friction surface chemistry. Moreover, the mechanism of the transfer film on the wear resistance and lubrication performance of the composites was also explored.

# 2 | EXPERIMENTAL SECTION

# 2.1 | Materials

Ti<sub>3</sub>AlC<sub>2</sub> was obtained from Jilin Eleven Technology Co., HF (AR) and Homophthalic dianhydride (PMDA, AR) were purchased from Shanghai Aladdin Materials, Co. Acetic

acid (AR) and 4,4'-oxydianiline (ODA, AR) were supplied by Shanghai Maclean Materials, Co. Tetraethyl orthosilicate (TEOS, AR) and ammonia (NH<sub>3</sub>·H<sub>2</sub>O, 25%–27%) were purchased from Anhui Zesheng Technology Co. Anhydrous ethanol (EtOH, AR) was obtained from Beijing Tongguang Fine Chemical Company.

# 2.2 | Preparation of $Ti_3C_2T_x@SiO_2$

The preparation details of  $Ti_3C_2T_x$  are shown in Supporting Information.<sup>19</sup> Based on the method in the literature, <sup>20</sup>  $Ti_3C_2T_x$ @SiO<sub>2</sub> was prepared as follows:  $Ti_3C_2T_x$  powder (0.20 g) was ultrasonically dispersed in a mixture of anhydrous ethanol (130 mL) and deionized water (25 mL). The above mixture was magnetically stirred in a flask and  $NH_3 \cdot H_2O$  (6 mL) was added dropwise until the pH of the solution was up to 10. TEOS (2 g) was

1002/pc.28200 by BEIJING INSTITUTION OF TECHNOLOGY, Wiley Online Library on [25/02/2024]

dissolved in anhydrous ethanol (20 mL) and the TEOS solution was added dropwise to the  $Ti_3C_2T_x$  dispersion with a dropwise acceleration of 1 drop/s. After the dropwise addition was completed, the temperature was raised to 35°C and the reaction was carried out for 4 h under magnetic stirring. When the reaction was finished, the above mixture was centrifuged several times and removed  $NH_3 \cdot H_2O$  and other by-products. Eventually, the sediment was dried under  $60^{\circ}C$  to capture the hybrids  $Ti_3C_2T_x@SiO_2$ .

# 2.3 | Fabrication of $Ti_3C_2T_x@SiO_2/PI$ composite film

The composite film was fabricated as follows: In the first step, PAA was prepared, and the process is shown in Supporting Information. In the second step,  $Ti_3C_2T_x@SiO_2$ 

was dispersed by *N*,*N*-dimethylacetamide and mixed with the prepared PAA (8 g) at room temperature. The mixture was stirred for 0.5 h and uniformly coated to 304 steel and dried for 4 h. The above samples were heated in a tube furnace to implement thermal iminization. (The temperature was  $100^{\circ}$ C,  $150^{\circ}$ C,  $200^{\circ}$ C,  $250^{\circ}$ C,  $300^{\circ}$ C and  $350^{\circ}$ C,  $2^{\circ}$ C/min.) The preparation procedure of  $Ti_3C_2T_x@SiO_2/PI$  is displayed in Figure 1. The name of  $Ti_3C_2T_x@SiO_2/PI$  samples is in Table S1.

# 2.4 | Characterization and measurement

X-ray diffraction (XRD) patterns were recorded with a D8 Advance diffractometer. The target material used was Cu and at a scanning speed of  $10^{\circ}/\text{min}$ .  $\text{Ti}_3\text{C}_2\text{T}_x\text{@SiO}_2$  and transfer film were characterized with Thermo ESCALAB 250XI x-ray photoelectron spectroscopy (XPS) and

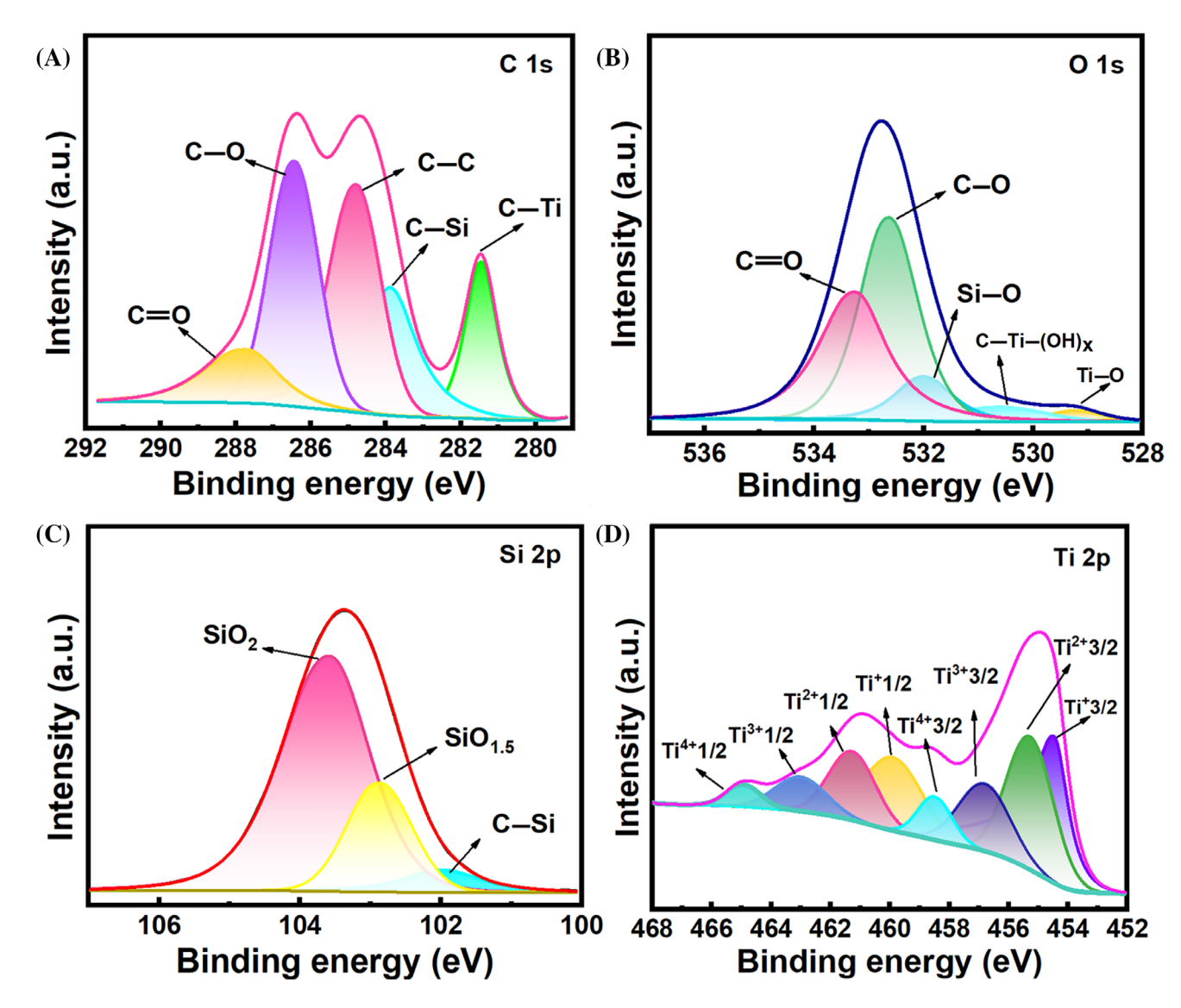


FIGURE 3 Elemental analysis of Ti<sub>3</sub>C<sub>2</sub>T<sub>x</sub>@SiO<sub>2</sub>. (A) C1s, (B) O1s, (C) Si2p, and (D) Ti2p.

LabRAM HR evolution Raman spectroscopy (the excitation wavelength was 633 nm.). Morphology and microstructures were observed with a Gemini 300 scanning electron microscope (SEM) and JEM-2100plus high-resolution transmission electron microscope (HRTEM). Atomic force microscope (AFM) analysis of composite surface morphology using Bruker's Dimension XR model. FT-IR test was obtained from a NICOLET IS10 Fourier transform infrared spectrometer (Nicolet, USA). Thermogravimetric analysis (TGA) of Ti<sub>3</sub>C<sub>2</sub>T<sub>x</sub>@SiO<sub>2</sub>/PI composites was collected by Shimadzu thermomechanical analysis system (The heating interval was 50-800°C, the heating rate was 10°C/min, N2 atmoball). The COF and wear rate of the samples were tested by the friction and wear tester model MS-M9000 (Lanzhou, China). Friction experiments were conducted at room temperature using a 4 mm diameter bearing steel (GCr15) ball as the upper counterpart ball, a cured PI composite as surface film, and a steel (304) disc as the underlying counter-facing plate. The rotating speed is 300 r/min, and the rotating radius is 3 mm. The normal load is 5 N, and the experimental duration is 30 min.

#### RESULTS AND DISCUSSION 3

# 3.1 | Structural analysis of hybrids $Ti_3C_2T_x@SiO_2$

The phase composition of hybrids was studied by x-ray diffraction and Raman spectroscopy. The intercalation of  $SiO_2$  between the  $Ti_3C_2T_x$  lamellae results in a shift of the

(002) diffraction peak to a lower angle with a decrease of 2θ (from 9.69° to 7.17°), which indicates the expansion of the layer spacing of Ti<sub>3</sub>C<sub>2</sub>T<sub>x</sub>. Meanwhile, diffraction peaks of amorphous  $SiO_2$  appeared near  $2\theta \approx 23^\circ$ , indicating that SiO<sub>2</sub> was successfully loaded on the Ti<sub>3</sub>C<sub>2</sub>T<sub>x</sub> lamellae (Figure 2A).<sup>21</sup> The FT-IR spectra show that four characteristic peaks about SiO2 appear in the curve of Ti<sub>3</sub>C<sub>2</sub>T<sub>x</sub>@SiO<sub>2</sub> compared to Ti<sub>3</sub>C<sub>2</sub>T<sub>x</sub> (Figure 2B). Specifically, the asymmetric telescopic and bending vibrations of Si-O-Si appear at 1093 and 472 cm<sup>-1</sup>, respectively. A characteristic peak of Si-OH at 947 cm<sup>-1</sup> and the stretching vibration of the Si-O bond at 797 cm<sup>-1</sup>. Therefore, the FT-IR spectra can also prove the successful loading of  $SiO_2$  on  $Ti_3C_2T_x$  nanosheets.<sup>22</sup>

The extent of defects in carbon materials can usually be reflected from Raman spectroscopy (Figure 2C). The D peak (1360 cm<sup>-1</sup>) is due to the sp<sup>3</sup> hybridization of graphene-like six-membered ring carbon atoms and represents defects, voids, and disorder in the carbon material. The G peak (1580 cm<sup>-1</sup>) is associated with the sp<sup>2</sup> hybridization of carbon atoms in graphene-like. The ratio  $I_{\rm D}/I_{\rm G}$  is used to express the degree of graphitization of carbon materials, where an increase in the ratio represents an increase in defects and disorder. <sup>23,24</sup> The  $I_{\rm D}/I_{\rm G}$  value of Ti<sub>3</sub>C<sub>2</sub>T<sub>x</sub> modified by SiO<sub>2</sub> increased from 0.72 to 0.92, indicating an increase in the degree of defects in the hybrids and a decrease in the percentage of ordered crystal structure, confirming the successful modification of Ti<sub>3</sub>C<sub>2</sub>T<sub>x</sub>.

The Ti<sub>3</sub>C<sub>2</sub>T<sub>x</sub>@SiO<sub>2</sub> hybrids were further analyzed by XPS to reveal the chemical composition. Compared to the full XPS spectrum of  $Ti_3C_2T_x$  (Figure S1), the full

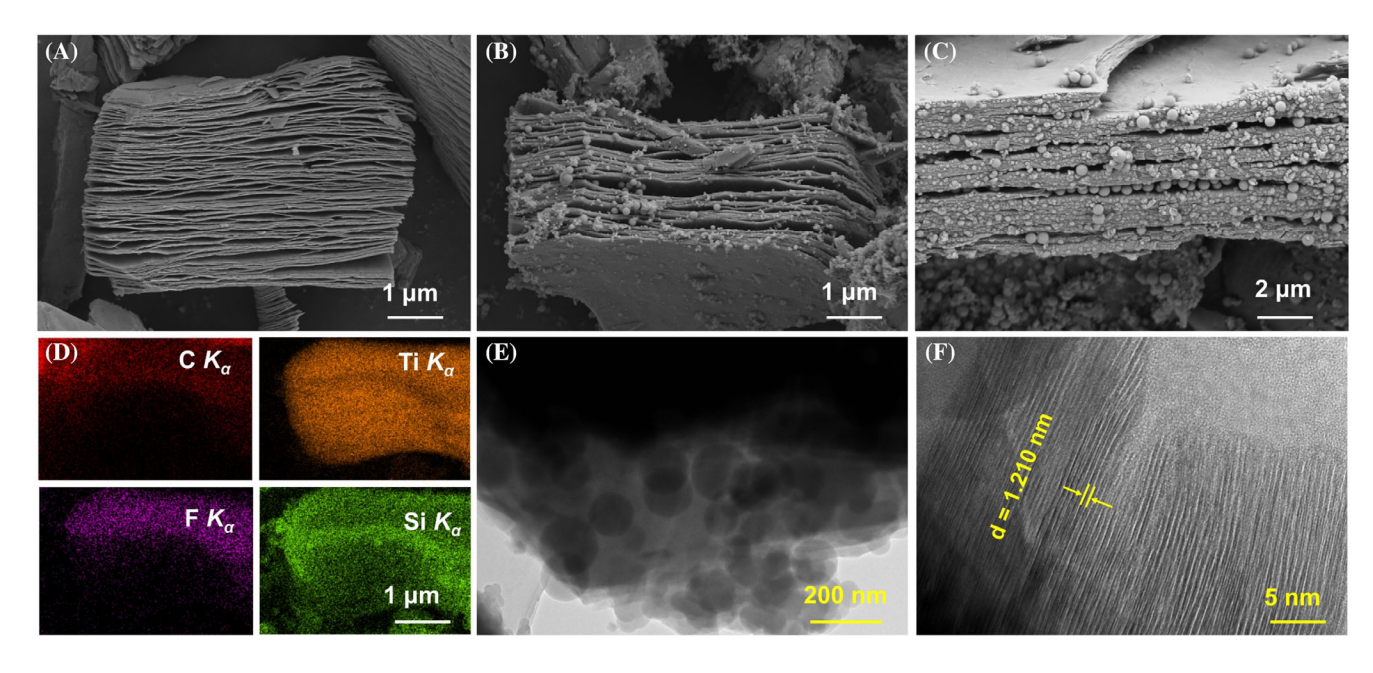


FIGURE 4 The SEM images of (A) Ti<sub>3</sub>C<sub>2</sub>T<sub>x</sub> and (B), (C) Ti<sub>3</sub>C<sub>2</sub>T<sub>x</sub>@SiO<sub>2</sub>. (D) EDS element mapping image of Ti<sub>3</sub>C<sub>2</sub>T<sub>x</sub>@SiO<sub>2</sub>. (E) TEM image and (F) HRTEM image of Ti<sub>3</sub>C<sub>2</sub>T<sub>x</sub>@SiO<sub>2</sub>.

om/doi/10.1002/pc.28200 by BEIJING INSTITUTION OF TECHNOLOGY, Wiley Online Library on [25/02/2024]. See the

spectrum (Figure 2D) and the fine spectrum (Figure 3C) of  $Ti_3C_2T_x@SiO_2$  show characteristic peaks of elemental Si, which is attributed to the fact that the  $SiO_2$  produced by the hydrolysis of TEOS has adhered to the  $Ti_3C_2T_x$  lamellae. The generation of C—Si bonds (Figure 3A). is mainly as a result of the interaction between  $Ti_3C_2T_x$  and  $SiO_2$  nanoparticles, the chemical bonding results in the solid "anchoring" of  $SiO_2$  on the surface of  $Ti_3C_2T_x$  or in the interlayers. Additionally, the three characteristic peaks appear at 101.8 eV, 102.9 eV, and 103.5 eV correspond to  $SiC_1$ ,  $SiO_1$ , and  $SiO_2$ , and the strong peak at 103.5 eV confirms the successful preparation of nano- $SiO_2$ .  $SiO_{1.5}$  corresponds to the formation of Si-O-Ti bonds (Figure 3B,C), which is due to the condensation

reaction between  $SiO_2$  and hydroxyl groups on the surface of  $Ti_3C_2T_x$  during the sol–gelation process. The Ti2p narrow spectrum in Figure 3D can be divided into  $Ti^+2p_{2/3}$  (454.7 eV),  $Ti^+2p_{1/2}$  (460.3 eV),  $Ti^{2+}2p_{2/3}$  (455.7 eV),  $Ti^{2+}2p_{1/2}$  (461.4 eV),  $Ti^{3+}2p_{3/2}$  (457.2 eV),  $Ti^{3+}2p_{1/2}$  (462.9 eV),  $Ti^{4+}2p_{3/2}$  (458.5 eV), and  $Ti^{4+}2p_{1/2}$  (464.7 eV) due to energy level splitting. The peaks of Ti-O bonds are shown at 460.3 and 464.7 eV, and the Ti—C bonds correspond to 462.9 eV.

Figure 4A shows an accordion-shaped multilayer  $Ti_3C_2T_x$ . After sol-gel hybridization,  $SiO_2$  nanoparticles are loaded on the surface of  $Ti_3C_2T_x$ , and some  $SiO_2$  is intercalated between the  $Ti_3C_2T_x$  layers (Figure 4B,C).  $SiO_2$  enlarges the layer spacing, which conforms with the XRD

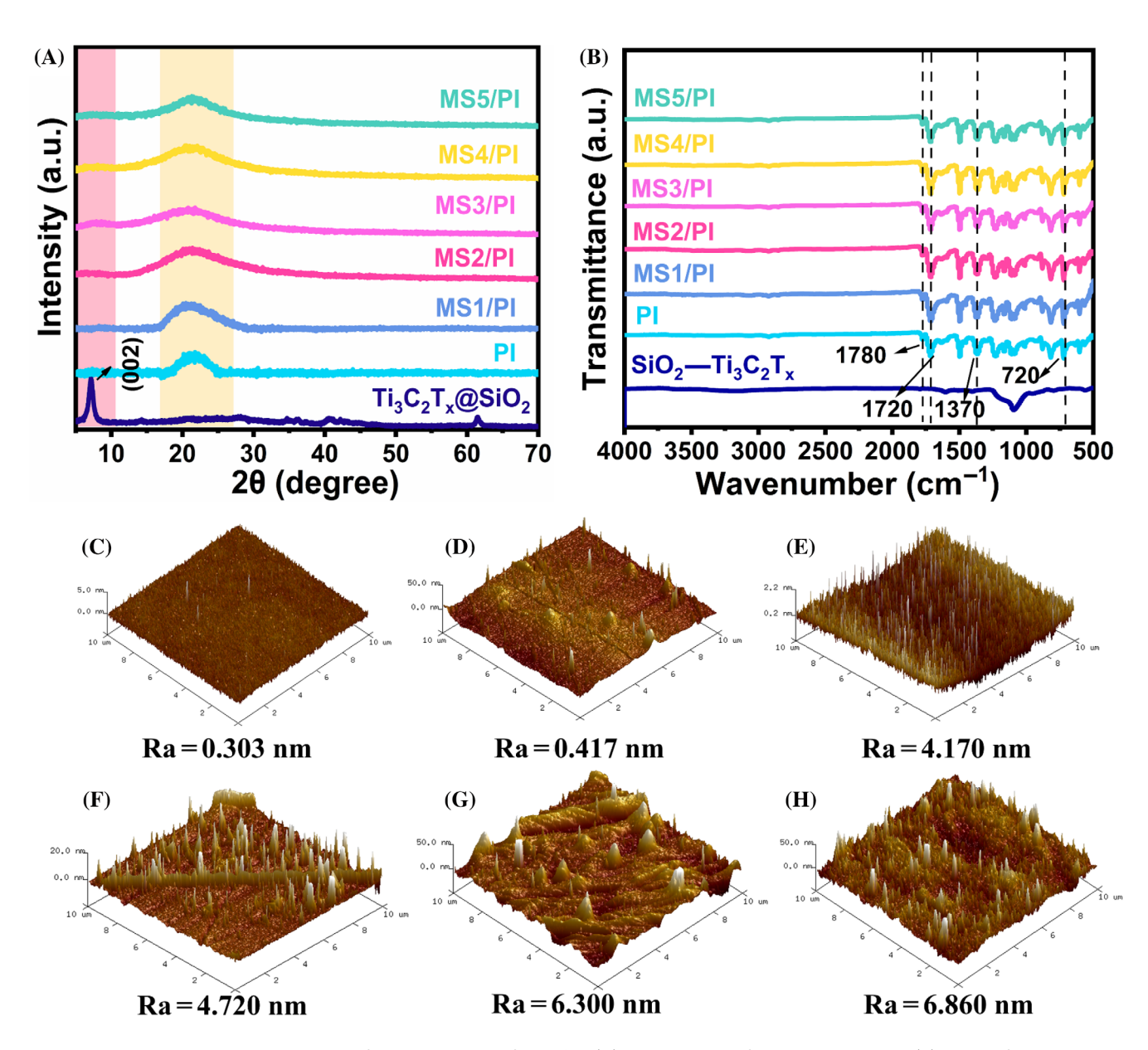


FIGURE 5 Chemical structure and surface morphology of samples. (A) XRD analysis of composite samples. (B) FT-IR of composite samples. (C) surface of polyimide. (D–H) the surface of composite samples.

patterns. The EDS images reflect the elemental distribution of  ${\rm Ti_3C_2T_x@SiO_2}$ , indicating the loading of  ${\rm SiO_2}$  on the  ${\rm Ti_3C_2T_x}$  surface (Figure 4D).  ${\rm SiO_2}$  nanoparticles grow on the surface of  ${\rm Ti_3C_2T_x}$  and between layers. The  ${\rm SiO_2}$  nanoparticles outside the lamellae have a larger particle size, and the particles formed between the layers are smaller. After intercalation, the lattice spacing of  ${\rm Ti_3C_2T_x}$  enlarged to about 1.210 nm, corresponding to the (002) crystalline surface, resulting in the enlarged layer spacing of  ${\rm Ti_3C_2T_x}$ .

# 3.2 | Friction properties

The composite samples were fabricated through the mixture of PAA and  $Ti_3C_2T_x@SiO_2$ . Polyimide and  $Ti_3C_2T_x@SiO_2/PI$  samples demonstrate characteristic peaks at  $2\theta \approx 22^\circ$ , which is attributed to the amorphous structure of polyimide (Figure 5A). The diffraction peaks of  $SiO_2$  and PI partially overlap and broaden, and a weak

diffraction peak appears near  $2\theta \approx 7.17^{\circ}$ , indicating that the PI matrix contains Ti<sub>3</sub>C<sub>2</sub>T<sub>x</sub>@SiO<sub>2</sub>. The chemical structure of polyimide and Ti<sub>3</sub>C<sub>2</sub>T<sub>x</sub>@SiO<sub>2</sub>/PI samples were tested by FT-IR (Figure 5B), which demonstrated the successful preparation of composite samples.<sup>27</sup> The Ti<sub>3</sub>C<sub>2</sub>T<sub>x</sub>@SiO<sub>2</sub>/PI composites have highly similar characteristic peaks with PI, indicating the introduction of Ti<sub>3</sub>C<sub>2</sub>T<sub>x</sub>@SiO<sub>2</sub> has a slight effect on thermal imidization. As shown in Figure 5C-H, the surface of polyimide is smooth. The hybrids create recessed or protruding structures on the surface of the composites, resulting in increased roughness. Specifically, the value of Ra reached 6.300 nm when Ti<sub>3</sub>C<sub>2</sub>T<sub>r</sub>@SiO<sub>2</sub> reached 2.00 wt% in Ti<sub>3</sub>C<sub>2</sub>T<sub>x</sub>@SiO<sub>2</sub>/PI composites. In addition, the hybrid Ti<sub>3</sub>C<sub>2</sub>T<sub>x</sub>@SiO<sub>2</sub> gives the material better thermal stability (Figure S2a,b).

The value of COF and wear rate are key indicators of a material's tribological properties. Low wear rates increase material life, and small COFs provide lubricating

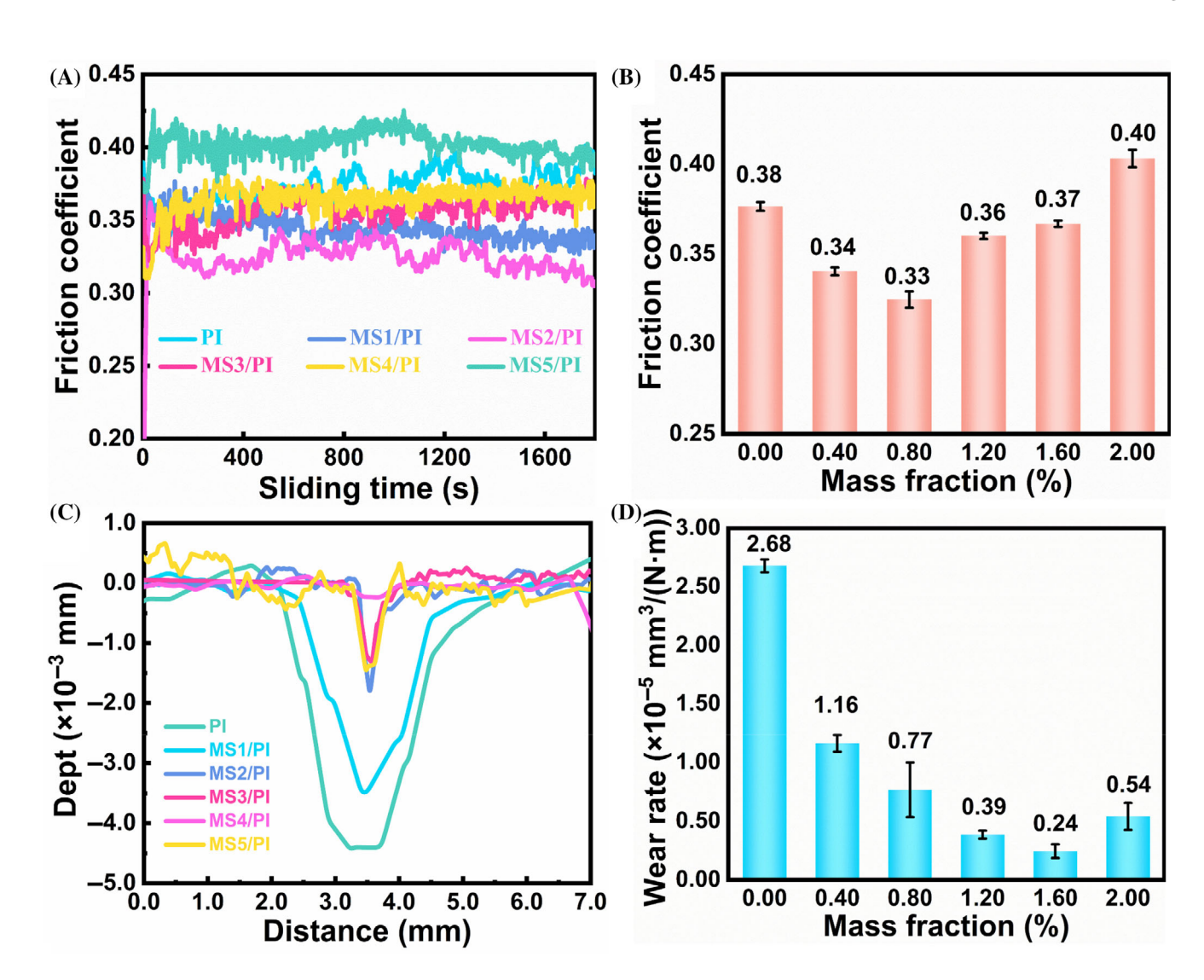


FIGURE 6 Friction properties of composite samples. (A) COF. (B) average value of COF. (C) abrasion depth. (D) wear rate.

/doi/10.1002/pc.28200 by BEIJING INSTITUTION OF TECHNOLOGY, Wiley Online Library on [25/02/2024]. See the Term

properties. Frictional heat also causes bonding of the polymer and thus deteriorates the lubrication properties. Ti<sub>3</sub>C<sub>2</sub>T<sub>x</sub>@SiO<sub>2</sub> effectively minimized the COF and wear rate. According to Figure 6, the COF decreased and then increased with the increase of the hybrid content in the composites. When Ti<sub>3</sub>C<sub>2</sub>T<sub>x</sub>@SiO<sub>2</sub> content was 0.80 wt%, the composites had the lowest average COF (0.33), which was 13.2% lower than the polyimide (Figure 6A,B). Similarly, the wear rate also shows a tendency to increase and then decrease with the addition of Ti<sub>3</sub>C<sub>2</sub>T<sub>x</sub>@SiO<sub>2</sub>. Moreover, the average wear rate was  $0.24 \times 10^{-5} \text{ mm}^3/(\text{N} \cdot \text{m})$  when  $Ti_3C_2T_x@SiO_2$  content was 1.60 wt%, which was 91.0% lower than polyimide (Figure 6C,D). This may be due to the fact that Ti<sub>3</sub>C<sub>2</sub>T<sub>x</sub>@SiO<sub>2</sub> can perform their lubricating and wear-resistant function better when their content is low, but once the optimal amount is exceeded, it will cause abrasive wear on the surface of the material, which is instead detrimental to the friction performance of the material. Overall, the superior friction reduction and anti-wear performance are owing to the function of Ti<sub>3</sub>C<sub>2</sub>T<sub>x</sub>@SiO<sub>2</sub>. In detail, the interlayer sliding of the Ti<sub>3</sub>C<sub>2</sub>T<sub>x</sub>@SiO<sub>2</sub> contributes to the lubricity of the composites. On the other hand, the presence of lamellar Ti<sub>3</sub>C<sub>2</sub>T<sub>x</sub> and SiO<sub>2</sub> further protects the polymer matrix from severe wear and tear. Moreover, the interface of composites also promotes stress transfer from the PI matrix to the Ti<sub>3</sub>C<sub>2</sub>T<sub>x</sub>@SiO<sub>2</sub>, which avoids stress concentration.<sup>28–30</sup>

8 WILEY—SPE INSPIRING PLASTICS PLASTICS

The abrasion of polyimide and composite samples were photographed using SEM. The abrasions of polyimide are wider and show deeper grooves (Figure 7A).

Ti<sub>3</sub>C<sub>2</sub>T<sub>x</sub> can narrow the abrasion marks of PI (Figure 7B-F). However, once the  $Ti_3C_2T_x@SiO_2$  addition exceeds 0.80 wt%, the roughness of the wear interface increases. This is because the excess Ti<sub>3</sub>C<sub>2</sub>T<sub>x</sub>@SiO<sub>2</sub> is exposed to the friction interface, which increases the roughness of the contact interface. Therefore, the increased roughness at the friction interface is a result of  $Ti_3C_2T_x@SiO_2$  wear.

#### Friction mechanism 3.3

During the friction process, the abraded material will transfer to the friction pair and form a transfer film. The topography of transfer film has a prominent influence on the friction performance of composites. To explore the friction reduction mechanism of Ti<sub>3</sub>C<sub>2</sub>T<sub>x</sub>@SiO<sub>2</sub> on PI substrate, the topography and elemental distribution were characterized by SEM (Figure 8A,B). From the EDS results, the Ti and Si elements originating from Ti<sub>3</sub>C<sub>2</sub>T<sub>x</sub>@SiO<sub>2</sub> are attached to the ball, indicating that the Ti<sub>3</sub>C<sub>2</sub>T<sub>x</sub>@SiO<sub>2</sub> transferred to the ball.

The ingredients of the transfer film were analyzed to explain the mechanism of friction reduction and antiwear from the perspective of friction chemistry. Therefore, we used XPS and Raman spectra to analyze the transfer film. Figure S3 mainly shows the C, N, O, Ti, and Si elements of the transfer film. Elements Ti and Si are derived from Ti<sub>3</sub>C<sub>2</sub>T<sub>x</sub>@SiO<sub>2</sub>. Figure 9A indicates a transfer of the composites to the steel ball under

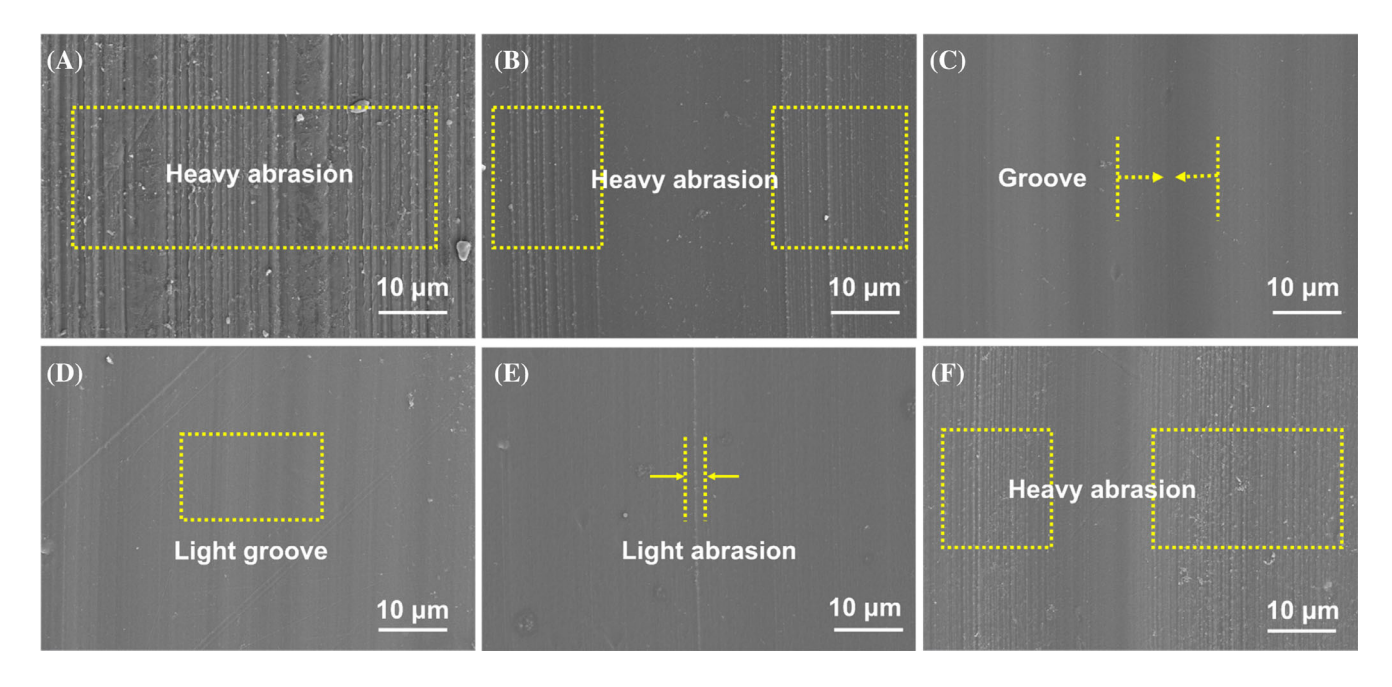


FIGURE 7 Abrasion scar morphology of the Ti<sub>3</sub>C<sub>2</sub>T<sub>x</sub>@SiO<sub>2</sub>/PI composites: (A) PI; (B) MS1/PI; (C) MS2/PI; (D) MS3/PI; (E) MS4/PI; and (F) MS5/PI.

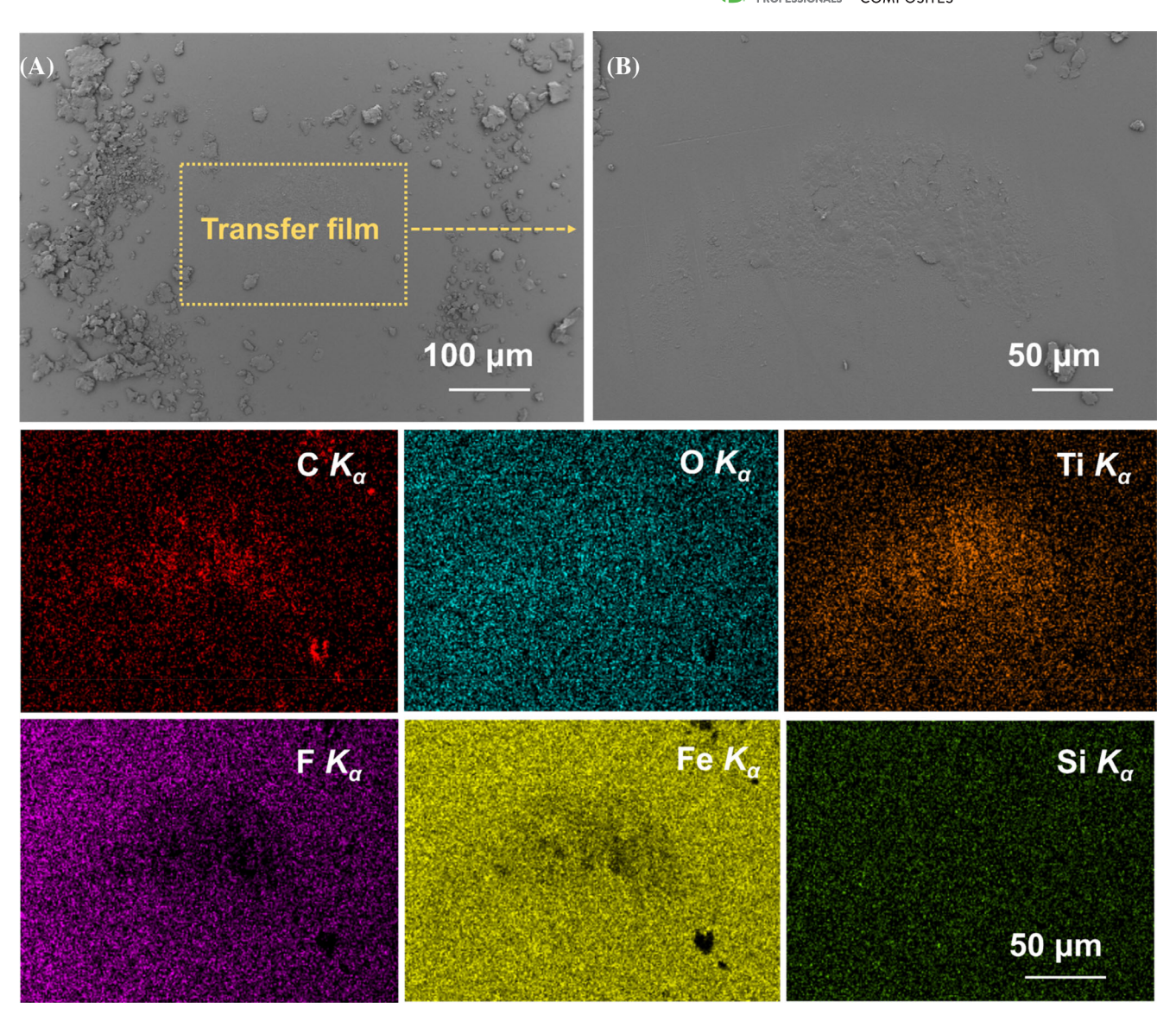


FIGURE 8 SEM image of Ti<sub>3</sub>C<sub>2</sub>T<sub>x</sub>@SiO<sub>2</sub>/PI composites friction spot and the EDS images: (A) transfer film; (B) partial enlargement.

frictional stress and frictional heat. The binding energies at 530.3 and 531.4 eV in Figure 9B, correspond to those at 710.6 and 725.2 eV in Figure 9D, representing the formation of the metal oxides Fe<sub>3</sub>O<sub>4</sub> and Fe<sub>2</sub>O<sub>3</sub>. This result suggests that oxidative reactions were induced to take place at high temperatures during friction. The peaks of Ti-O bonds are shown at 460.3 and 464.7 eV indicating that MXene is oxidized during friction. The narrow spectral peak shapes of Ti2p in the transfer film are similar to those of Ti<sub>3</sub>C<sub>2</sub>T<sub>x</sub>@SiO<sub>2</sub>, which may be attributed to the dehydration-condensation reaction of hydroxyl groups on the surface of Ti<sub>3</sub>C<sub>2</sub>T<sub>x</sub> with TEOS during friction (Figure 9C). SiO<sub>2</sub> is attached to the  $Ti_3C_2T_x$  functional groups, which mitigates the oxidation of Ti<sub>3</sub>C<sub>2</sub>T<sub>r</sub> to a certain extent. In addition, the signals of metal oxide  $Fe(CO)_x$  appear at 531.9 eV and 532.2 eV in the O1s narrow spectrum and 712.7 eV in the Fe2p narrow spectrum,

which is due to the chelating reaction between the  ${\rm Ti_3C_2T_x@SiO_2/PI}$  composites and ball under friction. The narrow spectra of Si 2p can also indicate that the transfer film contains  ${\rm SiO_2}$  (Figure 9E). Raman spectra show that the value of D/G of  ${\rm Ti_3C_2T_x@SiO_2}$  is 0.92, while the value of the D/G of the transfer film reaches 1.02 (Figure 9F). This increased ratio indicates a shift in the carbon composition of the transfer film towards an amorphous graphite structure and an increase in the degree of  ${\rm Ti_3C_2T_x@SiO_2}$  defects. The alternating ball-sheet structure of  ${\rm Ti_3C_2T_x@SiO_2}$  has good stress-carrying capacity and lubricity, which provides a good friction and wear reduction effect.

The principle of  $Ti_3C_2T_x@SiO_2$  improving friction performance of polyimide was shown in (Figure 10). During the friction, the composites peeled and tore under shear and friction stresses, generating lots of grinding debris. These abrasive debris containing  $Ti_3C_2T_x@SiO_2$ 

com/doi/10.1002/pc.28200 by BEIJING INSTITUTION OF TECHNOLOGY, Wiley Online Library on [25/02/2024]. See the Term

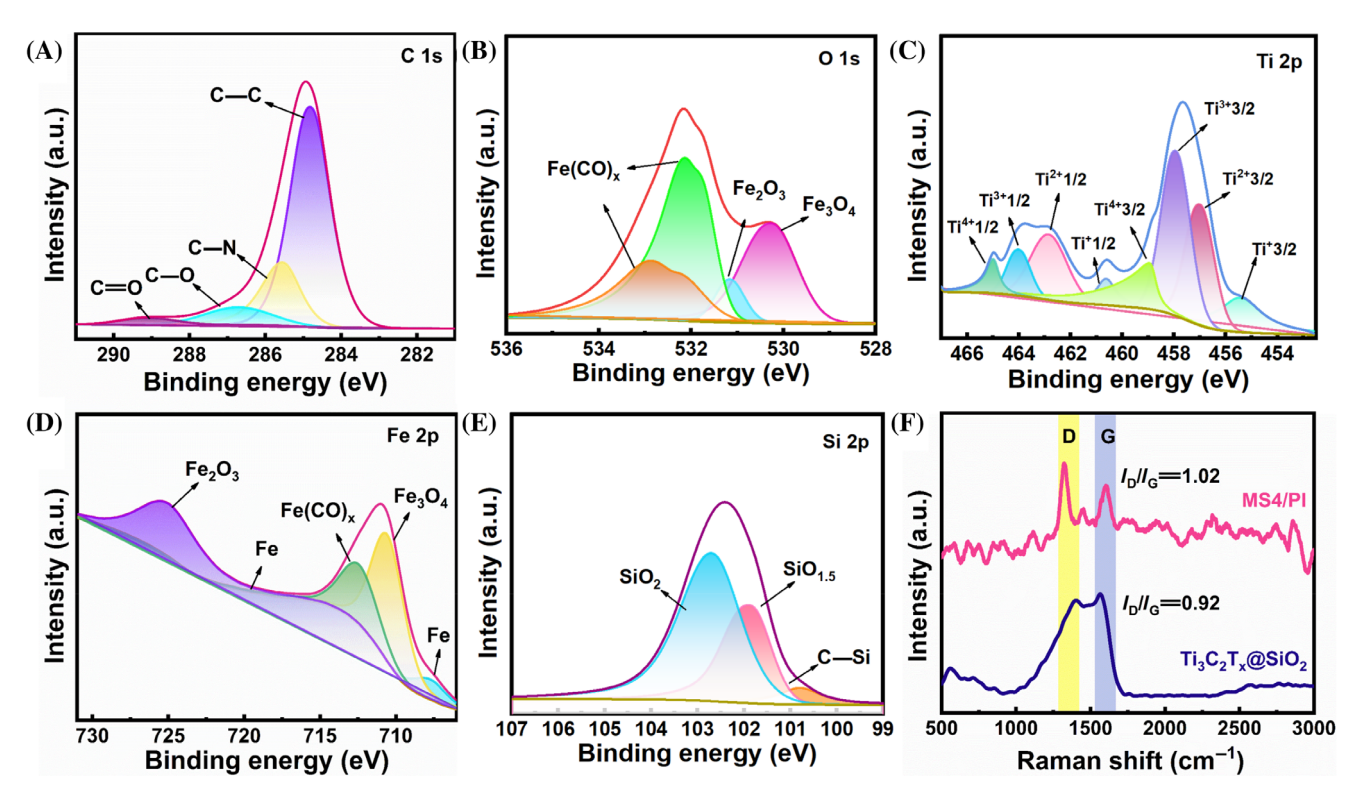


FIGURE 9 Analysis of transfer film (A-E) XPS narrow spectra of transfer film and (F) Raman analysis.

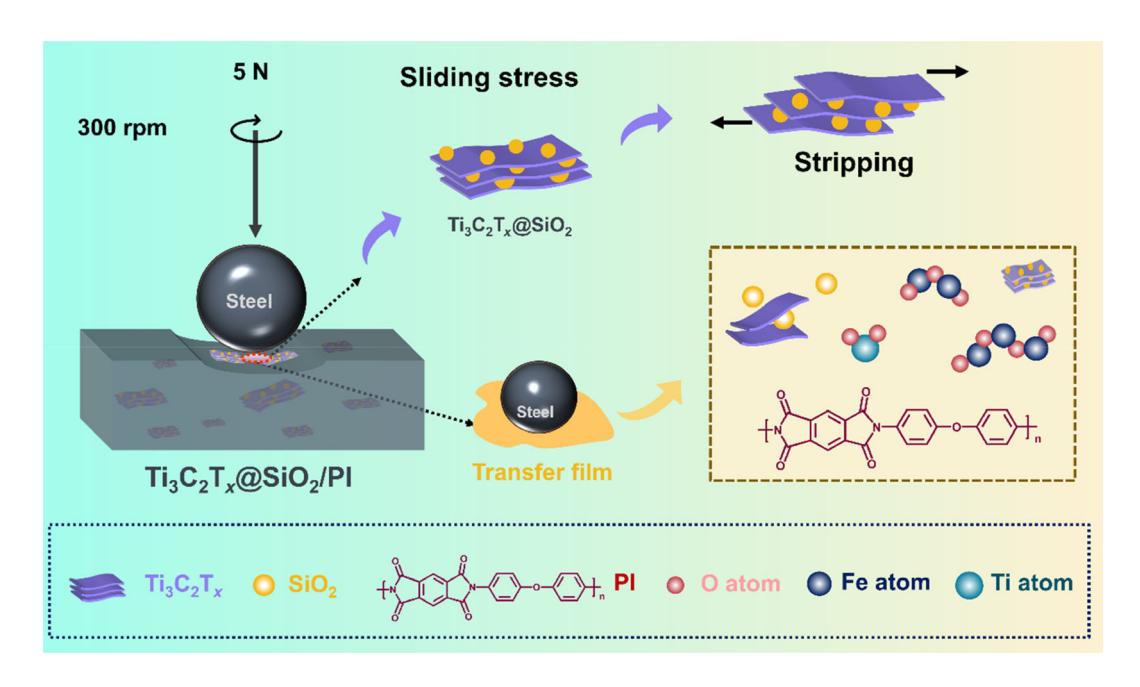


FIGURE 10 The mechanism of tribological property enhancement of PI by Ti<sub>3</sub>C<sub>2</sub>T<sub>x</sub>@SiO<sub>2</sub>.

hybrids, PI,  $Ti_3C_2T_x$ ,  $SiO_2$ ,  $TiO_2$ ,  $Fe_2O_3$ , and  $Fe_3O_4$ , adhere to the steel ball and create a transfer film. This transfer film separates the polymer matrix from the steel ball, effectively reducing the level of wear on the matrix. Specifically, frictional stress transfers along the PI matrix to  $SiO_2$ , and the energy transferred to  $SiO_2$  propagates along the chemical bonds to the  $Ti_3C_2T_x$  nanosheets.  $Ti_3C_2T_x$  is

stripped under stress, creating more energy dissipation paths and thus reducing the wear of the composites. The lamellae are peeled off easily because of the interpolated  $SiO_2$  between  $Ti_3C_2T_x$  lamellae. Spherical  $SiO_2$  changes the form of interfacial friction from sliding to rolling, thus relieving direct friction between the material and the steel ball and reducing the COF.<sup>31</sup> Moreover, unbonded  $SiO_2$ 

spheres can also transfer or dissipate frictional stress by sliding on  $Ti_3C_2T_x$  nanosheets. Therefore,  $Ti_3C_2T_x@SiO_2$  effectively improves the lubricating properties of PI.

# 4 | CONCLUSIONS

In this study, Ti<sub>3</sub>C<sub>2</sub>T<sub>x</sub>@SiO<sub>2</sub> hybrids were prepared by sol-gel method, and it was added into the PAA to fabricate Ti<sub>3</sub>C<sub>2</sub>T<sub>x</sub>@SiO<sub>2</sub>/PI samples with a method of thermal iminization. The intercalation of SiO<sub>2</sub> spheres between  $Ti_3C_2T_x$  sheets increases the layer spacing of  $Ti_3C_2T_x$ , which facilitates the exfoliation of the  $Ti_3C_2T_x$  sheets, thus improving the lubrication performance of the composites. In addition, the lowest COF of the composites is 0.33 when the content of  $Ti_3C_2T_x@SiO_2$  reaches 0.8 wt%. The  $Ti_3C_2T_x@SiO_2$  hybrids can also significantly improve the thermal stability and wear resistance of PI. The wear rate was 91.0% lower than that of PI when the content of  $Ti_3C_2T_x@SiO_2$  was 1.60 wt%. The unique structure of Ti<sub>3</sub>C<sub>2</sub>T<sub>x</sub>@SiO<sub>2</sub> facilitates the propagation and diffusion of sliding stresses from the PI matrix to the hybrids during friction. The hybrids, together with the PI matrix, tend to transfer to the surface of the steel ball to form a transfer film, which is an important factor in reducing the wear rate of the material. Therefore, the prepared Ti<sub>3</sub>C<sub>2</sub>T<sub>x</sub>@SiO<sub>2</sub> hybrids are effective solid lubricants and wear-resistant agents, which are potentially valuable for research in the field of improving the wear-resistant and lubricating properties of polymer materials.

# **AUTHOR CONTRIBUTIONS**

Guojing Chen: Conceptualization, Data curation, Investigation, Methodology, Project administration, Resources, Validation, Writing-original draft. Zhenqian Ma and Shuai jiang: Investigation, Methodology, Resources. Xinrui Wang and Yufei Huang: Investigation, Methodology. Chunpeng Chai: Conceptualization, Funding acquisition, Investigation, Methodology, Project administration.

# **ACKNOWLEDGMENTS**

In this work, some of the experiments were done at the Beijing Center for Applied Research in Radiation (XRD testing) and Tsinghua University (Raman spectroscopic testing). The authors would like to thank Shiyanjia lab (www.shiyanjia.com) for the support of SEM tests.

# CONFLICT OF INTEREST STATEMENT

The authors declare that they have no conflicts of interest to this work, and do not have any commercial or associative interest that represents a conflict of interest in connection with the work.

# DATA AVAILABILITY STATEMENT

Data will be made available on request from the authors.

### ORCID

*Chunpeng Chai* https://orcid.org/0000-0003-0334-9403

### REFERENCES

- Wang JL, Huang QY, Gao Y, et al. Molecular and atomic layer deposition of hybrid polyimide–Al<sub>2</sub>O<sub>3</sub> gate dielectrics for flexible electronic devices. *Chem Mater.* 2022;34:9119-9133.
- Zhang D, Wang TM, Wang QH, Wang C. Selectively enhanced oil retention of porous polyimide bearing materials by direct chemical modification. *J Appl Polym Sci.* 2017;134:45106.
- Xu ZX, Zhuang XD, Yang CQ, et al. Nitrogen-doped porous carbon superstructures derived from hierarchical assembly of polyimide nanosheets. Adv Mater. 2016;28:1981-1987.
- 4. Roy A, Mu LW, Shi YJ. Tribological properties of polyimide coating filled with carbon nanotube at elevated temperatures. *Polym Compos.* 2020;41:2652-2661.
- Ji RN, Wang SQ, Zou YC, et al. One-step fabrication of amorphous/ITO-CNTs coating by plasma electrolytic oxidation with particle addition for excellent Wear resistance. *Appl Surf Sci.* 2023;23:158274.
- Dong FX, Hou GL, Cao FX, Yan FY, Liu L, Wang JZ. The lubricity and reinforcement of carbon fibers in polyimide at high temperatures. *Tribol Int*. 2016;101:291-300.
- Zhao YL, Qi XW, Dong Y, et al. Mechanical, thermal and tribological properties of polyimide/Nano-SiO<sub>2</sub> composites synthesized using an in-situ polymerization. *Tribol Int.* 2016;103: 599-608.
- 8. Li N, Peng JH, Zhang P, Yue YZ. Amorphous MXene opens new perspectives. *Adv Mater*. 2023;35:2300067.
- Li XL, Luo H. Maximizing Terahertz Energy Absorption with MXene Absorber. Nano-Micro Lett. 2023;15:198.
- 10. Qian Y, Zhong J, Ou JP. Improvement in alkali-resistance of basalt fiber-reinforced polymer by  ${\rm Ti_3C_2T_X}$  (MXene) modified matrix. *Polym Compos.* 2023;44:2581-2591.
- Zhang H, Wang LB, Chen Q, et al. Preparation, mechanical and anti-friction performance of MXene/polymer composites. *Mater Des.* 2016;92:682-689.
- 12. Du CF, Wang ZJ, Wang XM, et al. Probing the lubricative behaviors of a high MXene-content epoxy-based composite under dry sliding. *Tribol Int.* 2022;165:107314.
- 13. Hao ZW, Zhou J, Liu D, et al. Two-dimensional confinement engineering of SiO<sub>2</sub> nanosheets supported Nano-cobalt for high-efficiency microwave absorption. *Chem Eng J.* 2023;473: 145296.
- Wu T, Jiang DE. Computational studies of MXenes. MRS Bull. 2023;48:253-260.
- 15. He S, Ruan CC, Shi YJ, et al. Insight to hydrophobic  $SiO_2$  encapsulated  $SiO_2$  gel: preparation and application in fire extinguishing. *J Hazard Mater*. 2021;405:124216.
- 16. He YP, Lin B, Wang YH, et al. Effect of homologous molecular crosslinking on the tribological properties of PTFE composites. *Polym Compos.* 2023;44:5132-5147.
- 17. Zhan MS, He J, Guo BY, Liu LH, Yu AB. Eulerian–Eulerian modeling of the formation and deposition of SiO2 in the outside vapor deposition process. *Chem Eng J.* 2022;449: 137783.

- 18. Zhang ZY, Kong DY, Li XF, Ao XL, Xiao XL. High temperature shape memory polymer with high Wear resistance. *Smart Mater Struct*. 2019;28:105005.
- 19. Grutzmacher PG, Suarez S, Tolosa A, et al. Superior Wearresistance of  ${\rm Ti_3C_2T_x}$  multilayer coatings. *ACS Nano*. 2021;15: 8216-8224.
- 20. Mu G, Mu DB, Wu BR, et al. Microsphere-like SiO<sub>2</sub>/MXene hybrid material enabling high performance anode for lithium ion batteries. *Small*. 2020;16:1905430.
- Zhou Y, Zhang SY, Zheng F, Lu QH. Intrinsically black polyimide with retained insulation and thermal properties: a black anthraquinone derivative capable of linear copolymerization.
  *Macromolecules*. 2021;54:9307-9318.
- 22. Wang NN, Wang H, Wang YY, et al. Robust, lightweight, hydrophobic, and fire-retarded polyimide/MXene aerogels for effective oil/water separation. *ACS Appl Mater Interfaces*. 2019;11:40512-40523.
- 23. Kiran NU, Deore AB, More MA, et al. Comparative study of cold electron emission from 2D Ti<sub>3</sub>C<sub>2</sub>T<sub>x</sub> MXene nanosheets with respect to its precursor Ti<sub>3</sub>SiC<sub>2</sub> MAX phase. *ACS Appl Mater Interfaces*. 2022;4:2656-2666.
- 24. Hu T, Wang JM, Zhang H, Li ZJ, Hu MM, Wang XH. Vibrational properties of  $Ti_3C_2$  and  $Ti_3C_2T_2$  (T= O, F, OH) Monosheets by first-principles calculations: a comparative study. *Phys Chem Chem Phys.* 2015;17:9997-10003.
- 25. Zhan YJ, Nan BF, Liu YC, et al. Multifunctional cellulose-based fireproof thermal conductive nanocomposite films assembled by in-situ grown  ${\rm SiO_2}$  nanoparticle onto MXene. *Chem Eng J.* 2021;421:129733.
- 26. He XL, Wu JX, Li SH, Chen Y, Zhang L, Sheng XX. In situ growth of aminated silica on MXene nanosheets: a novel 0D/2D hybrid structure for multifunctional waterborne epoxy composite coatings[J]. *Prog Org Coat*. 2022;171:107042.
- 27. Zhou L, Qi HM, Lei Y, Yu JX, Guo BG, Zhang D. Ti<sub>3</sub>C<sub>2</sub> MXene induced high tribological performance of polyimide/polyurea

- copolymer at a wide temperature range. *Appl Surf Sci.* 2023; 608:155157.
- 28. Chen GJ, Fu WY, Liu ZQ, et al. Self-sealing polyurethane coatings containing high oil-absorption resin for storage facility and fuel pipelines. *Prog Org Coat*. 2022;166:106789.
- Xiong M, Xiong L, Xiong K, Liu F. A new strategy for improvement of Interface and mechanical properties of carbon fiber/epoxy composites by grafting graphene oxide onto carbon fiber with hyperbranched polymers via thiol-ene click chemistry. *Polym Compos.* 2023;44:5490-5498.
- Nie YX, Zhou XY, Dong LS, et al. Synergistic dispersion and Tribo-film formation of liquid metal @graphene oxide/epoxy coating: toward improved mechanical and anti-wear properties. *Polym Compos.* 2023;44:4815-4825.
- Wu JY, Liu H, Wang HD, Ma W, Wang TM, Wang QH. Effects of TiO<sub>2</sub> decorated reduced graphene oxide on mechanical and tribological properties of thermosetting polyimide, compos. *Interfaces*. 2022;29:985-998.

# SUPPORTING INFORMATION

Additional supporting information can be found online in the Supporting Information section at the end of this article.

How to cite this article: Chen G, Ma Z, Jiang S, Wang X, Huang Y, Chai C. Highly lubricating and wear-resistant  $\text{Ti}_3\text{C}_2\text{T}_x\text{@SiO}_2/\text{PI}$  composites based on the action of transfer film at the friction surface. *Polym Compos.* 2024;1-12. doi:10.1002/pc.28200